PERFORMANCE OF A P-I-N DIODE AS A RECOIL PROTON SPECTROMETER

S. Agosteo[1,2], C. Birattari[2,3], G. D'Angelo [1,2], F. Dal Corso[4], A. Foglio Para [1], I. Lippi[4], A. Pola[1,2], P. Zotto[4,5].

[1] Dipartimento di Ingegneria Nucleare, Politecnico di Milano, via Ponzio 34/3, 20133 Milano, Italy.

[2] INFN, Sezione di Milano, via Celoria 16, 20133 Milano, Italy.

[3] Dipartimento di Fisica, Università degli Studi di Milano, via Celoria 16, 20133 Milano, Italy.

[4] INFN, Sezione di Padova, via Marzolo 8, 35131 Padova, Italy.

[5] Dipartimento di Fisica, Politecnico di Milano, piazza Leonardo da Vinci 32, 20133 Milano, Italy.

ABSTRACT

A prototype recoil-proton spectrometer consisting of a commercial p-i-n diode coupled with a polyethylene converter was developed and tested. The response functions of the detector were measured with mono-energetic neutron beams. The response functions were also determined analytically and with Monte Carlo simulations using the FLUKA code. The effect of secondary charged particles produced by thermal and fast neutron interactions in the silicon diode was also investigated. Spectral measurements were performed for secondary neutrons generated by 5 MeV protons striking a thick beryllium target. The reconstructed neutron spectrum was compared with data taken from the literature, giving satisfactory results. The use of the proposed prototype is limited by the contribution of photons to the response to fast neutrons.

KEYWORDS

P-I-N diode, neutron spectrometry, neutrons.

PACS: 29.30.H, 29.40.W

Corresponding author:
Stefano Agosteo
Dipartimento di Ingegneria Nucleare
Politecnico di Milano
Via Ponzio 34/3
20133 Milano, Italy
tel: +39 02 2399 6318
fax: +39 02 2399 6309
e-mail: stefano.agosteo@polimi.it

1. Introduction

Silicon devices are currently employed for fast neutron detection, usually exploiting the recoil-protons generated in hydrogenated materials covering their surface. Diodes coupled with recoil-proton converters were also proposed for individual neutron dosimetry [1-6]. The present work investigates the possibility of using this detection technique for neutron spectrometry, as was preliminarily discussed in ref. [7]. It should be mentioned that this technique was successfully employed for the spectrometry of neutrons generated by deuterium-tritium plasmas [8-9].

The recoil-proton spectrometer discussed herein consists of a windowless p-i-n photodiode 0.5 mm thick (Hamamatsu S3509-06) coupled with a polyethylene radiator (1 mm thick). The diode sensitive area is 9x9 mm^2. The electronic chain uses standard modules, namely a charge sensitive preamplifier (Hamamatsu H4083), a spectroscopy amplifier (Silena 7614) and an ADC converter (EG&G Ortec ADCAM 926).

The response functions of the device to mono-energetic neutrons were determined both theoretically (analytically and with Monte Carlo simulations) and experimentally in the energy interval from 0.5 MeV to 5 MeV. The maximum detectable energy is determined by the thickness of the totally depleted layer, which should match with the maximum range of the recoil-protons in silicon. The totally depleted layer of the p-i-n diode employed in this work is 300 μm thick, corresponding to the range of 6 MeV protons in silicon.

An unfolding code based on an iterative technique was developed for this spectrometer. The spectra of nominal mono-energetic neutrons and the one of the secondary neutrons generated at 0° by 5 MeV protons striking a thick beryllium target were unfolded applying this code. The spectrum obtained for the p-Be interaction was compared with the results of ref. [10].

The response to direct neutron interactions of the bare p-i-n diode (i.e., without the plastic radiator) was also investigated in order to determine its influence on the detector performance.

The small sensitive area of this detector should guarantee a spatial resolution much better than the one achievable with systems based on neutron moderation (e.g. Bonner spheres) and comparable to the one provided by superheated bubble detectors. A possible application could be for example the assessment of neutron spectra in the proximity of critical organs of an anthropomorphic phantom for radiation protection purposes.

It should be emphasized that the present spectrometer is a prototype, based on a commercial device, which is characterized by a limited range of detectable neutron energies. Possible improvements of its performance are also discussed.

2. Response as a proton-recoil spectrometer

As already mentioned, the recoil-proton spectrometer was realized placing a 1 mm thick polyethylene layer in contact with the silicon diode.

The relation between the energy of the incident neutrons and that deposited in the diode is not univocal, since the device can also detect recoil-protons generated at scattering angles different from zero. The maximum detectable angle depends on the point of elastic interaction in the converter. Moreover, the recoil-protons can lose part of their energy in the polyethylene converter before interacting with the diode and the energy resolution of the detector contributes to disperse farther the primary information. Therefore, the knowledge of the response functions of the detector to mono-energetic neutrons is fundamental for the reconstruction of the spectrum of the primary neutrons. These response functions were measured in mono-energetic neutron fields and a simple theoretical model was also developed in order to explain their behaviour.

The effect of the diode bias voltage (i.e. of the thickness of the depletion layer) on the response functions was also investigated.

3.1 Experimental measurements

The spectrometer, biased at different voltages, was irradiated at the Van De Graaff accelerator of the INFN Legnaro National Laboratories (LNL, Legnaro, Italy) with 4.8 MeV mono-energetic neutrons generated by 6.5 MeV protons striking a thin LiF target. The investigated energy corresponds to the maximum value which can be achieved with the LNL Van De Graaff through the ^{7}Li(p,n) reaction. The results are shown in Fig. 1.

The response curves show a pronounced decrease from low to intermediate energies followed by a smoother distribution which extends up to the maximum energy deposited in the depletion layer. The smooth region up to the maximum deposited energy is due to recoil protons generated in the radiator. At low energies, the response is completely overwhelmed by low LET events, due to secondary photons and X rays generated in the LiF target, in the detector assembly and in the environment. This limits the lower detectable energy of the spectrometer. The photon component lowers decreasing the thickness of the depletion layer,

but on the other hand a thinner depletion layer imposes a limitation on the maximum detectable energy.

The edge corresponding to the maximum deposited energy shifts towards higher values while decreasing the bias voltage. From 0 to -5 V a pronounced saturation edge can be observed, suggesting that the range of the incident protons is higher than the depletion layer thickness.

At bias voltages lower than –15 V (down to –70 V), the depletion layer becomes deep enough to stop all the recoil protons and indeed these spectra do not show a relevant shift. Capacitance measurements showed that the depletion layer at –15 V is about 160 μm thick. The range of 4.8 MeV protons in silicon is about 200 μm and therefore there is an indication that there is charge collection also from the doped silicon bulk, to be related to the field funnelling effect [11]. This effect is due to a local distortion of the electric field in the depletion layer, induced by high-LET particles, leading to the collection of electron-hole pairs produced in the substrate. The effective thickness of the active region is thus increased with respect to the one of the depletion layer.

The curves shown in Fig. 1 led to set the bias voltage at –15 V. This value allows to characterize the prototype detector up to the maximum neutron energy which can be delivered by the LNL Van De Graaff and to minimize the contribution of low-LET events. The response functions resulting from irradiation with monoenergetic neutrons of several energies generated with the reaction ^{7}Li(p,n)^{7}Be are shown in Fig. 2. The photon background overwhelms the proton signal at energies below about 1.2 MeV

2.2 Theoretical modelling

Monte Carlo simulations of the detector response functions were performed with the FLUKA code [12-15]. The simulation geometry consisted of a polyethylene converter 1 mm thick placed in contact with a silicon layer 300 μm thick. The source was a parallel beam of mono-energetic neutrons. The response function (i.e. the number of recoil-protons depositing their energy in the detector per unit neutron fluence) is shown in Fig. 3 for 2.7 MeV neutrons, together with the corresponding experimental data. The distribution of secondary photons is not observable, since the LiF target assembly, the detector case and the accelerator hall were not simulated. The agreement of the simulation results with measurements is satisfactory also for all the other neutron energies considered.

The response functions of the spectrometer were also determined analytically for parallel beams of mono-energetic neutrons. The polyethylene radiator was considered thicker than the range of the recoil protons of maximum energy, which is equal to that of the impinging neutrons (E_n) in a head-on collision. Therefore, only secondary protons generated in a useful polyethylene layer adjacent to the diode surface can be detected.

The range-energy relation in polyethylene was described with a power law, derived fitting the data available in ref. [16]:

$$R_p = R_0\left(\frac{E_{p,0}}{MeV}\right)^{\beta} \tag{1}$$

where R_p is the range of the recoil protons in the polyethylene radiator, R_0 is a constant value with the same units of R_p (≈ 20 μm in polyethylene with density ρ = 0.93 g cm^{-3}), ß is dimensionless (about 1.75 for proton energies from a few hundreds of keV up to a few MeV) and $E_{p,0}$/MeV is the ratio of the initial energy of the scattered proton to the unit energy in MeV. The energy (MeV) of protons slowing-down in polyethylene will be indicated as E_p in the following.

The function (1) can be obtained expressing the proton stopping power as:

$$-\frac{dE_p}{dx} = \frac{1}{\beta R_0 E_p^{\beta-1}} \tag{2}$$

and integrating $-dE_p/dx$ from zero to R_p, (or from $E_{p,0}$ to 0 in terms of energy).

The path X_r, travelled by a proton not completely stopped in the polyethylene radiator is:

$$X_r = \int_0^{X_r} dx = \int_{E_d}^{E_{p,0}} \frac{dE_p}{-dE_p/dx} = \beta R_0 \int_{E_d}^{E_{p,0}} E_p^{\beta-1} dE_p = R_0 E_{p,0}^{\beta} - R_0 E_d^{\beta} \tag{3}$$

where E_d is the energy of the proton leaving the radiator, which, in the present case, is equal to the energy transferred to the detector (E_d=$E_{p,0}$ – E_r, being E_r the energy transferred to the radiator).

E_d can be determined from expression (3) as:

$$E_d = \left(E_{p,0}^{\beta} - \frac{X_r}{R_0} \right)^{\frac{1}{\beta}} \text{ MeV} \qquad (4)$$

In the case of recoil-protons generated in elastic collisions with neutrons, $E_{p,0}=E_n \cdot \cos^2\theta$, where θ is the angle between the direction of the impinging neutron (assumed to be perpendicular to the detector surface) and that of the recoil-proton. Expressing the path travelled by the recoil-proton in the radiator as $X_r = h/\cos\theta$, where h is the distance between the point of elastic interaction in polyethylene and the detector surface, the energy deposited in the diode results:

$$E_d = \left[\left(E_n \cos^2 \theta \right)^{\beta} - \left(\frac{h}{R_0 \cos\theta} \right) \right]^{\frac{1}{\beta}} \text{ MeV} \qquad (5)$$

It should be underlined that the path of the recoil-proton in the detector does not appear in expression (4), since it was assumed that protons are completely absorbed in the detector and that the energy deposited in silicon is computed by difference between total proton energy and energy lost in the radiator. Under this hypothesis, the detector material is irrelevant for calculating E_d. This also allows to determine expression (4) in an alternative way, by considering a dummy detector in polyethylene and therefore referring to the same values of R_0 and β. A similar approach is described in ref. [18] for a ΔE-E silicon detector. The path X_d travelled by a recoil-proton in the polyethylene detector is thus given by $R_0 \cdot E_d^{\beta}$ and coincides with $X_d = R_p - X_r = R_0 \cdot E_{p,0}^{\beta} - h/\cos\theta$. Again, $E_d = [E_{p,0}^{\beta} - h/(R_0 \cdot \cos\theta)]^{1/\beta}$.

Expression (4) indicates a strong non-linearity between E_d and $E_{p,0}$; for instance a proton of $E_{p,0}$ = 1 MeV generated in polyethylene at 20 μm from the detector is completely stopped in the converter and thus E_d = 0, while a proton generated at the same distance with $E_{p,0}$ = 2 MeV deposits an amount of energy E_d = 1.64 MeV in the detector.

Expression (5) holds if neutron interactions with carbon nuclei in polyethylene and the Coulomb scattering of recoil-protons in the converter are assumed to be negligible.

The spectral distribution $p(E_d)$ of the energy E_d deposited in the diode was calculated by assuming that: i) the interaction probability of neutrons is uniform inside the very thin useful layer of polyethylene of thickness R_p; ii) the angular distribution of the recoil protons is uniform with respect to a $\cos^2\theta$ law (i.e. the elastic scattering is isotropic in the centre-of-mass

system). Thus, $E_{p,0}$ is uniform in the interval (0 – E_n). Under these approximations $p(E_d)$ can be expressed as:

$$p(E_d) = \frac{2}{3}\beta \frac{E_d^{\beta-1}}{E_n^{\beta}}\left[1-\left(\frac{E_d}{E_n}\right)^{\frac{3}{2}}\right] \qquad (6)$$

It should be underlined that expression (6**)** refers to one interacting neutron and that the fraction of detected protons results to be 1/(ß +3/2).

The agreement between the theoretical model and the experimental results can be checked fitting expression (6) to the data acquired with mono-energetic neutrons. Assuming an exponential trend for the photon background, the fitting function is:

$$N(E_d) = e^{(a+b\cdot E_d)} + c\cdot p(E_d) \qquad (7)$$

where c is a normalization constant. The function fits correctly the experimental spectra as shown in Fig 4.

In expression (7), the parameter β in $p(E_d)$ fixes the function shape, while E_n corresponds to the neutron spectrum end-point, since it is equivalent to the maximum energy deposited by the recoil-protons in the diode. Therefore, E_n provides an intrinsic energy calibration of the diode. The fitted values of E_n provide the linear calibration function:

$$E_d(keV) = 2.784 \times ADCchannel + 15.16 \qquad (8)$$

The parameter β shows an energy dependence on the experimental data while being rather stable on the simulated data. Results are plotted in Fig. 5. The disagreement between the simulated and the experimental data may be due to instrumental effects which were not considered in the Monte Carlo calculations. The model is nonetheless successful in providing a set of functions which describes correctly the experimental spectra and can be used for unfolding the neutron spectrum in a non-monochromatic situation. A detailed derivation of expression (6) is reported in ref. [17], together with its modification in the case of a radiator thickness lower than R_p.

3. Unfolding of experimental data

The experimental responses to nominal mono-energetic neutrons (Fig. 2) were used to test the unfolding procedure. Only the upper part of the energy spectra of the recoil-protons was considered (thus excluding the contribution of photons) and unfolded. A standard iterative technique, aiming at reducing the experimental χ^2 starting from a distribution uniform in energy, was employed for this purpose. The response matrix was composed by a set of functions $p_j(E_d)$ (j=1,N) determined with expression (6) for N different values of E_n. For a quantitative evaluation, the functions $p_j(E_d)$ were multiplied by the corresponding probability π_j of generating a recoil-proton in the converter per unit neutron fluence. This probability is given by $\pi_j=\sigma(E_n)\cdot N_H\cdot R_p\cdot S$, where: i) $\sigma(E_n)$ is the elastic scattering cross section for neutrons of energy E_n on hydrogen, which can be parameterised as $[4.83/(E_n)^{0.5}– 0.578]$ (in barn) [18] for 0.3 MeV < E_n <30 MeV, ii) N_H is the number of hydrogen nuclei in the converter per unit volume, iii) R_p results from expression (1) and iv) S is the detector sensitive area (0.9x0.9 cm^2).

For ideal mono-energetic neutrons (i.e. with an energy distribution described by a Dirac δ-function), the experimental response is described by:

$$R_j = \pi_j\left[p_j(E_d) \otimes f(E_d)\right] \qquad (9)$$

where $f(E_d)$ is the normalized resolution function of the diode (e.g a gaussian function). In the case of nearly mono-energetic neutrons, any deviation from R_j has to be attributed to the energy spread of the energy distribution. The consistency of the curves fitting the experimental data in Fig. 4 indicates that the energy spread of the nominal mono-energetic neutron spectra should be rather limited.

The spectral fluences resulting from unfolding the data related to the irradiation with nominal mono-energetic neutrons are shown in Fig. 6 for three different neutron energies. The same figure shows the experimental data normalized to the total charge of accelerated protons impinging on the LiF target. The responses calculated by fitting the analytical set of functions $p_j(E_d)$ to the experimental data are also plotted.

The FWHM of the unfolded peaks resulted to be about 140 keV, 160 keV and 200 keV at 2.7, 3.5 and 4.3 MeV, respectively. It should be underlined that these FWHMs include the spread of the energy distribution of the neutron beams used for calibration (unknown a-priori) and the energy resolution of the spectrometer. The energy resolution (FWHM) of the detector was measured with alpha-particles from a thin natural-uranium source and resulted to

be 140 keV and 160 keV at 4.20 and 4.77 MeV, respectively. Thus the energy spread of the nominal mono-energetic neutrons should be of the order of a few percent.

The capability of resolving continuous neutron spectra was also checked. To this aim, the energy distribution of secondary neutrons generated at 0° by 5 MeV protons striking a thick beryllium target was measured at the LNL**.** The resulting energy distribution of the neutron yield above 1 MeV is compared in Fig. 7 with data measured with time of flight techniques [10]. The guess distribution for the iterative unfolding procedure was uniform in energy. The unfolded spectrum agrees quite satisfactorily with the reference data above 1.5 MeV. The discrepancy in the energy interval 1.0-1.5 MeV may be ascribed to the detection of low-LET particles generated by photon interactions in the device. The peak at about 2.7 MeV resulted to be about 30% higher than that measured in ref. [10]. It should be underlined that the normalization uncertainty (detector positioning, beam charge, etc.) of the present measurements may be assessed around 20-30%.

4. Direct response of p-i-n diode to neutrons

A set of measurements was carried out to study possible effects due to the charged particles produced directly by neutrons on silicon and on the doping nuclei. These effects could modify the response functions and bias the spectra measured with the detector. The diode was irradiated without the plastic radiator with both thermal and fast neutrons. The bias voltage was set at 0 V, to minimize the contribution of photons.

4.1 Thermal neutron irradiations

Thermal neutrons mainly interact with boron, used as a p-type dopant in semiconductors. The relevant reaction is $^{10}B(n,\alpha)^{7}Li$ with a cross section of about 3800 b. The Q-value of the reaction on ^{10}B is 2.79 MeV and ^{7}Li is produced in an excited state with a branching ratio of 94%. Therefore, in most of cases, the available energy is shared among the α-particle (1.47 MeV), the ^{7}Li ion (0.84 MeV) and a gamma ray (0.48 MeV). It should be noted that 0.48 MeV gamma ray has a very low probability of interacting with the diode.

The diode was irradiated in the thermal column of the TAPIRO reactor (ENEA-Casaccia, Rome, Italy). The spectrum of the energy deposited in the diode is shown in Fig. 8. Three peaks can be observed in the figure:

- *a low-energy peak*, which may be attributed to the total energy deposition of ^{7}Li and the partial energy deposition of the α-particle in the diode depletion layer;

- *a mid-energy peak*: which may be attributed to the total energy deposition of the α-particle and the partial energy deposition of ^{7}Li;
- *a high-energy peak*: total energy deposition of both ^{7}Li and α-particle (2.31 MeV). This peak can be fitted by a gaussian function centred at 2.19±0.06 MeV.

A Monte Carlo algorithm was set up to verify the assumptions listed above. The simulation generates and transports the reaction products inside the silicon detector. The angular distribution of ^{7}Li and of the α-particle was assumed isotropic and Coulomb multiple scattering was neglected. The stopping power of the reaction products in silicon was calculated with the SRIM-2000 code [19-20].

The p-i-n diode is characterized by an intrinsic (i) silicon zone sandwiched between a very thin p^+ layer and a n^+ layer. The depletion layer is located below the p^+-i junction and extends within the intrinsic zone when the bias voltage is increased. Boron is essentially contained in the p^+ zone. Therefore, from the point of view of the collection of the electron-hole pairs, the structure of the diode shows a region containing a large quantity of boron (partially active, i.e. in the p^+ zone included in the depletion layer), an intrinsic region partially active (corresponding to the largest part of the depletion layer), a passive intrinsic region and a passive n^+ region.

The simulation of the real situation would have required the accurate knowledge of the size of the active region doped with boron and its doping profile. Since this information was unavailable, only a qualitative approach was carried out, assuming that the doped region was rather thin (of the order of 1 μm) and uniformly doped.

The simulated spectra of the deposited energy are shown in Fig. 9. Different sizes of the active and passive regions were considered, and the results agree qualitatively with the experimental spectrum shown in Fig. 8, thus supporting the proposed interpretation.

The ^{10}B reaction rate was estimated to be about 2.2×10^{-6} s^{-1} per unit fluence rate of thermal neutrons, while that due to recoil-protons is of the order of a few 10^{-5} s^{-1} per unit fluence rate of fast neutrons. Therefore, the effect of thermal neutrons on the detector response can be limited to negligible values only if the ratio of the thermal neutron fluence rate to that of fast neutrons is low. It should be underlined that the fluence rate of thermal neutrons was more than a factor 10^2 lower than that of fast neutrons during the calibration of the detector with monoenergetic neutrons and the measurements related to the ^{9}Be(p,n) reaction.

4.2 Fast neutron irradiations

Observable events are mainly due to fast neutron interactions with the silicon nuclei, since the reaction cross sections of the dopants are of the same of order of magnitude than those of silicon and the latter is obviously more abundant. Elastic scattering should not give rise to detectable signals up to a few MeV, since the maximum recoil energy of silicon is about 13% of that of the impinging neutrons. Therefore, the most important reactions should be $^{28}Si(n,\alpha)^{25}Mg$ and $^{28}Si(n,p)^{28}Al$ with threshold energies of 2.75 MeV and 4 MeV, respectively.

The diode was irradiated with mono-energetic neutrons generated at the LNL. The deposited energy spectra obtained from several neutron energies are shown in Fig. 10. The size of the depletion layer (about 20 μm at zero bias voltage) is not large enough to stop the reaction products. Hence, the peak visible at higher energies is due to a saturation effect and corresponds to the maximum energy deposited in the depletion layer.

The detector cross section of the n + ^{28}Si reaction can be computed subtracting the low energy distribution associated to the photon background to the spectra shown in Fig. 10. Fig. 11 shows this cross section when limiting the calculation to deposited energy $E_d > 1$ MeV. A tentative extrapolation to lower deposited energies (to compute the cross section for any deposited energy value) suggests a 10% upward correction, but with an unknown systematic error. Both the visual inspection of the deposited energy spectra (Fig. 10) and the cross section rise (Fig. 11) show a threshold at an incident neutron energy of about 3 MeV. The measured cross section is one order of magnitude lower than the one for the recoil-protons generated from neutron scattering in the converter. The distortion of the spectra should therefore be rather limited. It should be emphasized that the analytical response functions do not take into account the effect of direct neutron interactions on silicon. The fact that they proved to be consistent with the experimental responses at the investigated neutron energies is another indication of the minimal impact of direct neutron interactions. On the other hand, the use of the experimental response functions (which include anyway the contribution of direct fast neutron interactions) should ensure that the unfolded neutron spectra are not affected by these events.

5. Conclusions

The response functions of the neutron spectrometer, based on a p-i-n diode, were characterized both experimentally and analytically. The effects due to direct neutron

interactions with the silicon device and the doping materials (mainly boron) were also investigated. It should be underlined that the charged particles generated by thermal neutron capture on ^{10}B may affect the response functions of the spectrometer in the presence of intense thermal neutron fields. This effect can be reduced by shielding the device with thermal neutron absorbing materials. In this case, the contribution of photons to the detector response may increase, because of the generation of prompt gamma rays (e.g when using a cadmium shield). An alternative way is to discriminate the ^{10}B reaction products through pulse-shape analysis.

The energy threshold for fast neutron reactions on the silicon device was observed at about 3 MeV. The contribution of these threshold-interactions is obviously included in the measured response functions of the spectrometer. Therefore, any further correction is not required when the experimental response functions are used to unfold the experimental data.

The minimum detectable energy of the spectrometer is limited by the energy deposited by low LET events generated by secondary photons. The possibility of reducing the detection limit by discriminating photons from recoil-protons through the pulse rise-time is under investigation. The rejection of the photon contribution is also necessary to attenuate the contribution of prompt gamma rays when the device has to be shielded against thermal neutrons.

In conclusion, the prototype proposed in the present work was useful to demonstrate the feasibility of a recoil-proton spectrometer based on a p-i-n diode. This device can assess fast neutron spectra only in very controlled situations (e.g. with associated thermal neutron fields of low intensity) and in a limited energy interval (1.0-5.0 MeV). Pulse-shape discrimination is strongly necessary to minimize the contribution of photons and to improve the accuracy of the reconstructed neutron spectra.

ACKNOWLEDGMENTS

This work was funded by INFN and the Italian Ministry for University and Research. The constant support of the operators of the LNL Van De Graaff and of TAPIRO reactor is fully acknowledged. The authors wish to thank prof. Thomas N. Massey (Ohio University, Athens, Ohio) for providing numerical data of the secondary neutron spectra from $^{9}Be(p,n)$.

REFERENCES

[1] J.M. Bordy, T. Lahaye, F. Landre, C. Hoflack, S. Lequin, J. Barthe, *Single Diode Detector for Individual Neutron Dosimetry Using a Pulse Shape Analysis*, Radiat. Prot. Dosim. 70 (1-4) (1997) 73-78.

[2] J.C. Vareille, et al., *Advanced Detectors for Active Neutron Dosimeters*, Radiat. Prot. Dosim. 70 (1-4) (1997) 79-82.

[3] F. Fernandez, E. Luguera, C. Domingo, C. Baixeras, *Separation of the Neutron Signal from the Gamma Component in (n-γ) Fields Using Differential Pulse Analysis Techniques with a Double Silicon Diode*, Radiat. Prot. Dosim. 70 (1-4) (1997) 87-92.

[4] T. Moiseev, *Study of a Moderator Type Electronic Neutron Dosimeter for Personal Dosimetry*, Radiat. Prot. Dosim. 70 (1-4) (1997) 93-96.

[5] M. Luszik-Bhadra, W.G. Alberts, E. Dietz, B.R.L. Siebert, *Feasibility Study of an Individual Electronic Neutron Dosimeter*, Radiat. Prot. Dosim. 70 (1-4) (1997) 97-102.

[6] M. Luszik-Bhadra, *A Prototype Personal Neutron Dosimeter with One Silicon Diode*, Radiat. Prot. Dosim. 96 (1-3) (2001) 227-229.

[7] S. Agosteo, A. Castoldi, L. Castellani, P. Colautti, G. D'Angelo, L. De Nardo, A. Favalli, I. Lippi, R. Martinelli, G. Tornielli, P. Zotto, *A Feasibility Study of a Single Event Spectrometer Based on Semiconductor Devices, Radiation Protection Dosimetry*, in press.

[8] N.P. Hawkes, D.S. Bond, V. Kiptily, O.N. Jarvis, S.W. Conroy, *Neutron Spectrometry for D-T Plasmas in JET, Using a Tandem Annular-Radiator Proton-Recoil Spectrometer*, Nucl. Instrum. Meth. A476 (2002) 490-494.

[9] N.P. Hawkes, D.S. Bond, S. Croft, O.N. Jarvis, A.C. Sherwood, *The design of a Proton Recoil Telescope for 14 MeV Neutron Spectrometry*, Nucl. Instrum. Meth. A476 (2002) 506-510.

[10] W.B. Howard, S.M. Grimes, T.N. Massey, S.I. Al-Quraishi, D.K. Jacobs, C.E. Brient, J.C. Yanch, *Measurement of the Thick-Target ^{9}Be(p,n) Neutron Energy Spectra*, Nucl. Sci. Engineering 138(2) (2001) 145-160.

[11] C.M. Hsieh, P.C. Murley, R.R. O'Brien, *A Field-Funneling Effect on the Collection of the Alpha-Particle-Generated Carriers in Silicon Devices*, IEEE Electron Device Letters, EDL-2 (1981) 103-105.

[12] A. Fassò, A. Ferrari, J. Ranft and P.R. Sala, *FLUKA: Present Status and Future Developments*, Proceedings IV Int. Conference on Calorimetry in High Energy Physics,

La Biodola, Italy, 21-26 September 1993, Ed. A. Menzione and A. Scribano, World Scientific (1994) p. 493-502.

[13] A. Ferrari and P.R. Sala, *The Physics of High Energy Reactions*, Proceedings of the Workshop on Nuclear Reaction Data and Nuclear Reactors Physics, Design and Safety, International Centre for Theoretical Physics, Miramare-Trieste, Italy, 15 April-17 May 1996, Eds. A. Gandini and G. Reffo, Vol. 2, World Scientific (1998) 424-532.

[14] A. Fassò, A. Ferrari, J. Ranft and P.R. Sala, *An update about FLUKA*, Proceedings 2nd Workshop on Simulating Accelerator Radiation Environments, CERN, Geneva, Switzerland, 9-11 October 1995, Ed. G.R. Stevenson, CERN Divisional Report TIS-RP/97-05 (1997) p. 158-170.

[15] A. Fassò, A. Ferrari, J. Ranft and P.R. Sala, *New Developments in FLUKA Modelling Hadronic and EM Interactions*, Proceedings 3rd Workshop on Simulating Accelerator Radiation Environments, KEK, Tsukuba, Japan 7-9 May 1997, Ed. H. Hirayama, KEK Proceedings 97-5 (1997) p. 32-43.

[16] J. F. Janni, *Proton Range-Energy Tables, 1 keV-10 GeV*, Atomic Data and Nuclear Data Tables 27 (1982) 147-339.

[17] S. Agosteo, A. Foglio Para, *Metrology and spectrometry of neutrons in the MeV range by standard photodiodes*, Proceedings of SIMAI 2002, VI Congresso Nazionale della Società Italiana di Matematica Applicata e Industriale (Chia, Italy, 27-31 maggio 2002), available on CD-ROM.

[18] G.F. Knoll, Radiation Detection and Measurement (third edition), John Wiley and Sons, New York (2000).

[19] J.F. Ziegler, J.P. Biersack, *SRIM 2000*, IBM (1999), www.srim.org.

[20] J.F. Ziegler, J.P. Biersack, U. Littmark, *The Stopping and Range of Ions in Solids*, Pergamon Press, New York, 1985.

FIGURE CAPTIONS

Fig. 1 Effect of the bias voltage on the response function of the spectrometer irradiated with 4.8 MeV mono-energetic neutrons. Expression (8) was applied for energy calibration.

Fig. 2 Response functions of the spectrometer irradiated with mono-energetic neutrons of several energies generated at the LNL Van De Graaff. E_n is energy of the incident neutrons. Expression (8) was applied for energy calibration.

Fig. 3 FLUKA simulation of the spectrometer response function for 2.7 MeV neutrons compared to the corresponding experimental curve. Expression (8) was applied for the energy calibration of the experimental curve.

Fig. 4 Analytical and experimental response functions for several neutron energies. The fitting curves (solid lines) are described by expression (6).

Fig. 5 The values of the β parameter resulting from fitting the experimental and the simulated data.

Fig. 6 a) Unfolded spectral fluences (histogram, solid line) of mono-energetic neutrons generated at 0° from a thin lithium fluoride target bombarded with protons of several energies; b) experimental spectra of the recoil-protons normalized to the charge of accelerated protons striking the LiF target (open circles); c) responses calculated by fitting the analytical set of functions $p_j(E_d)$ to the experimental data (dotted line). E_n is the expected peak energy of the mono-energetic neutrons.

Fig. 7 Yield of neutrons generated at 0° by 5 MeV protons striking a thick beryllium target. The spectrum obtained unfolding the data collected with the spectrometer discussed in this work is compared with the one measured in ref. [10].

Fig. 8 Spectral distribution of the energy deposited (E_d) in the diode irradiated in the thermal column of the TAPIRO reactor.

Fig. 9 Monte Carlo simulation of the spectral distribution of the energy deposited (E_d) in the active region of the diode by the charged particles produced by thermal neutrons via the reaction $^{10}B(n,\alpha)^7Li$. The results refer to different sizes of the active and the passive region of the diode (see text).

Fig. 10 Spectral distribution of the energy deposited in the diode by charged particles generated in silicon by interactions of neutrons of different energies.

Fig. 11 Detector cross section of the $n+^{28}Si$ reaction calculated for deposited energies above 1 MeV.

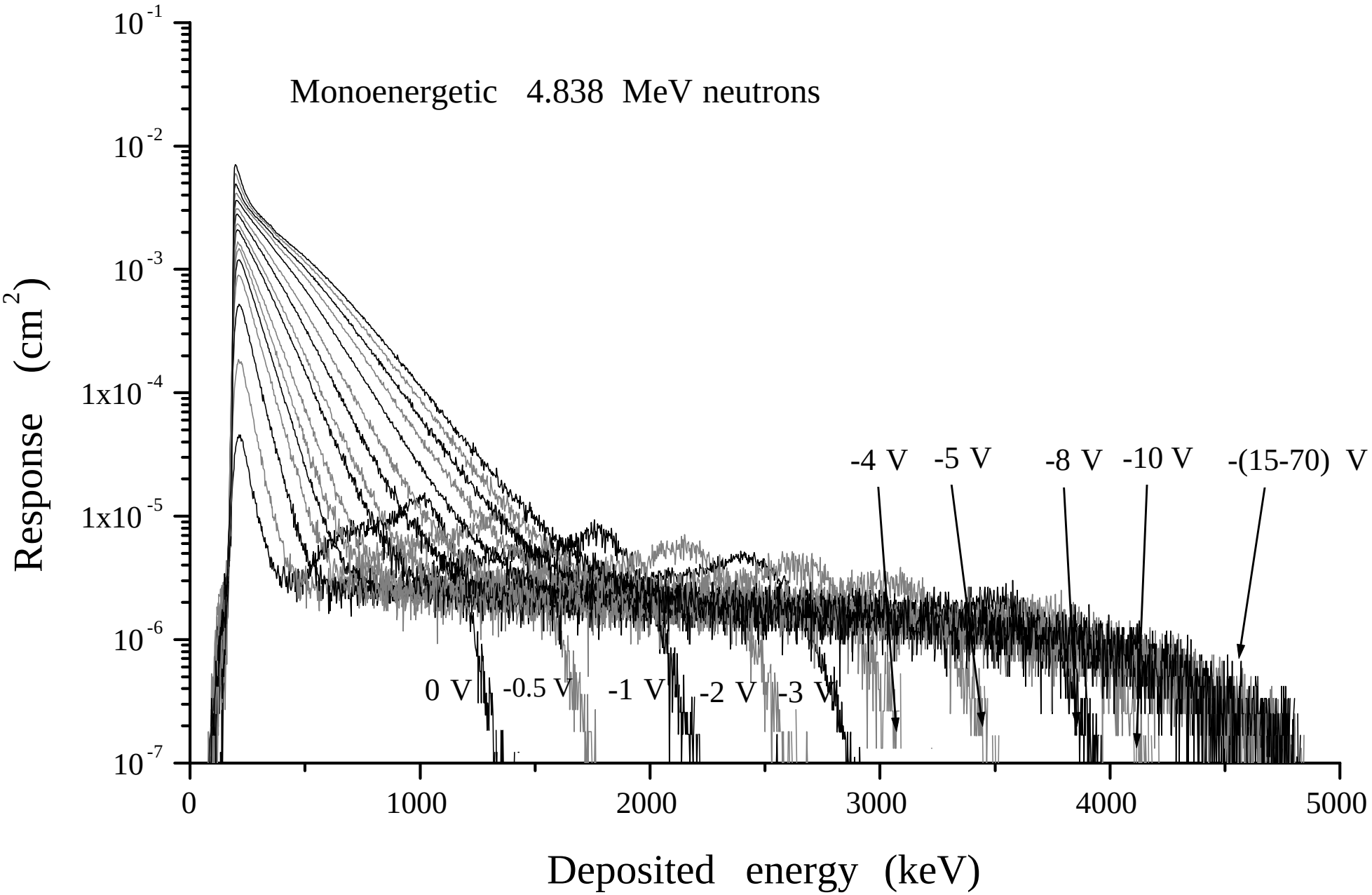
Monoenergetic 4.838 MeV neutrons
Response (cm^2)
10^{-1}
10^{-2}
10^{-3}
1x10^{-4}
1x10^{-5}
10^{-6}
10^{-7}
0 V
-0.5 V
-1 V
-2 V
-3 V
-4 V
-5 V
-8 V
-10 V
-(15-70) V
0
1000
2000
3000
4000
5000
Deposited energy (keV)

Figure 1

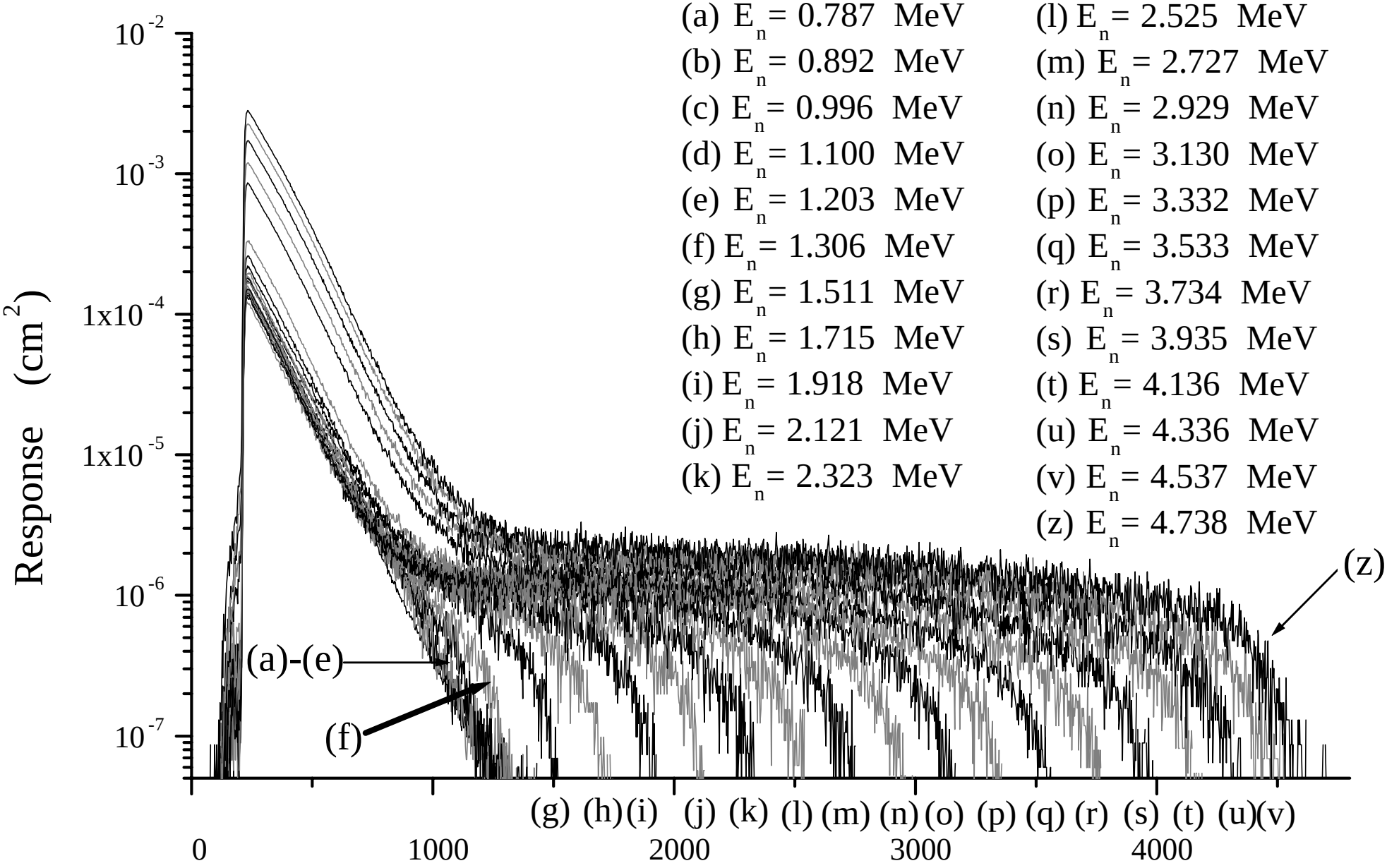
(a) E_n = 0.787 MeV
(b) E_n = 0.892 MeV
(c) E_n = 0.996 MeV
(d) E_n = 1.100 MeV
(e) E_n = 1.203 MeV
(f) E_n = 1.306 MeV
(g) E_n = 1.511 MeV
(h) E_n = 1.715 MeV
(i) E_n = 1.918 MeV
(j) E_n = 2.121 MeV
(k) E_n = 2.323 MeV
(l) E_n = 2.525 MeV
(m) E_n = 2.727 MeV
(n) E_n = 2.929 MeV
(o) E_n = 3.130 MeV
(p) E_n = 3.332 MeV
(q) E_n = 3.533 MeV
(r) E_n = 3.734 MeV
(s) E_n = 3.935 MeV
(t) E_n = 4.136 MeV
(u) E_n = 4.336 MeV
(v) E_n = 4.537 MeV
(z) E_n = 4.738 MeV
Response (cm^2)
10^{-2}
10^{-3}
1x10^{-4}
1x10^{-5}
10^{-6}
10^{-7}
(a)-(e)
(f)
(z)
(g) (h) (i) (j) (k) (l) (m) (n) (o) (p) (q) (r) (s) (t) (u) (v)
0
1000
2000
3000
4000
Deposited energy (keV)

Figure 2

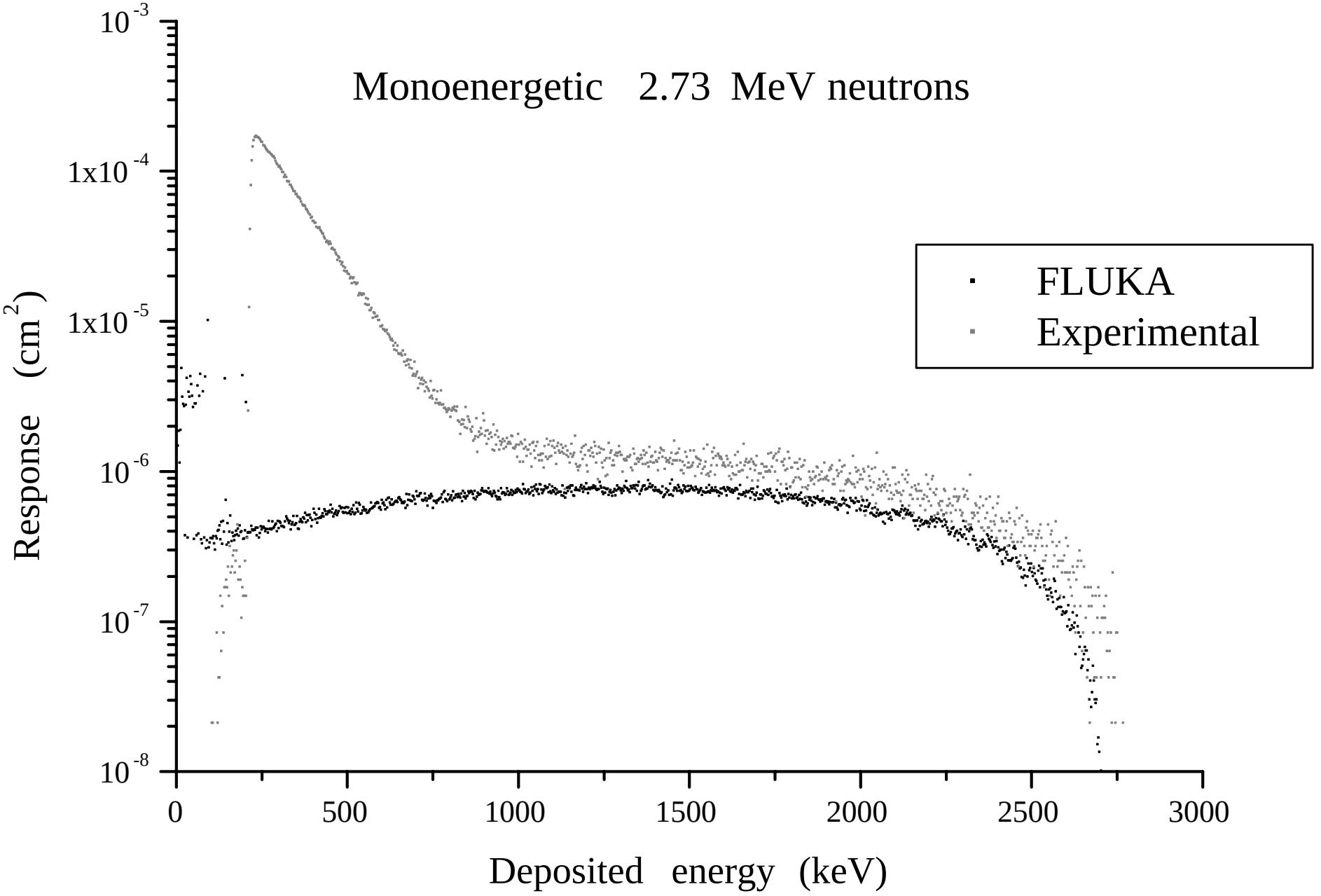
Monoenergetic 2.73 MeV neutrons
FLUKA
Experimental
Response (cm^2)
10^{-3}
$1x10^{-4}$
$1x10^{-5}$
10^{-6}
10^{-7}
10^{-8}
0
500
1000
1500
2000
2500
3000
Deposited energy (keV)

Figure 3

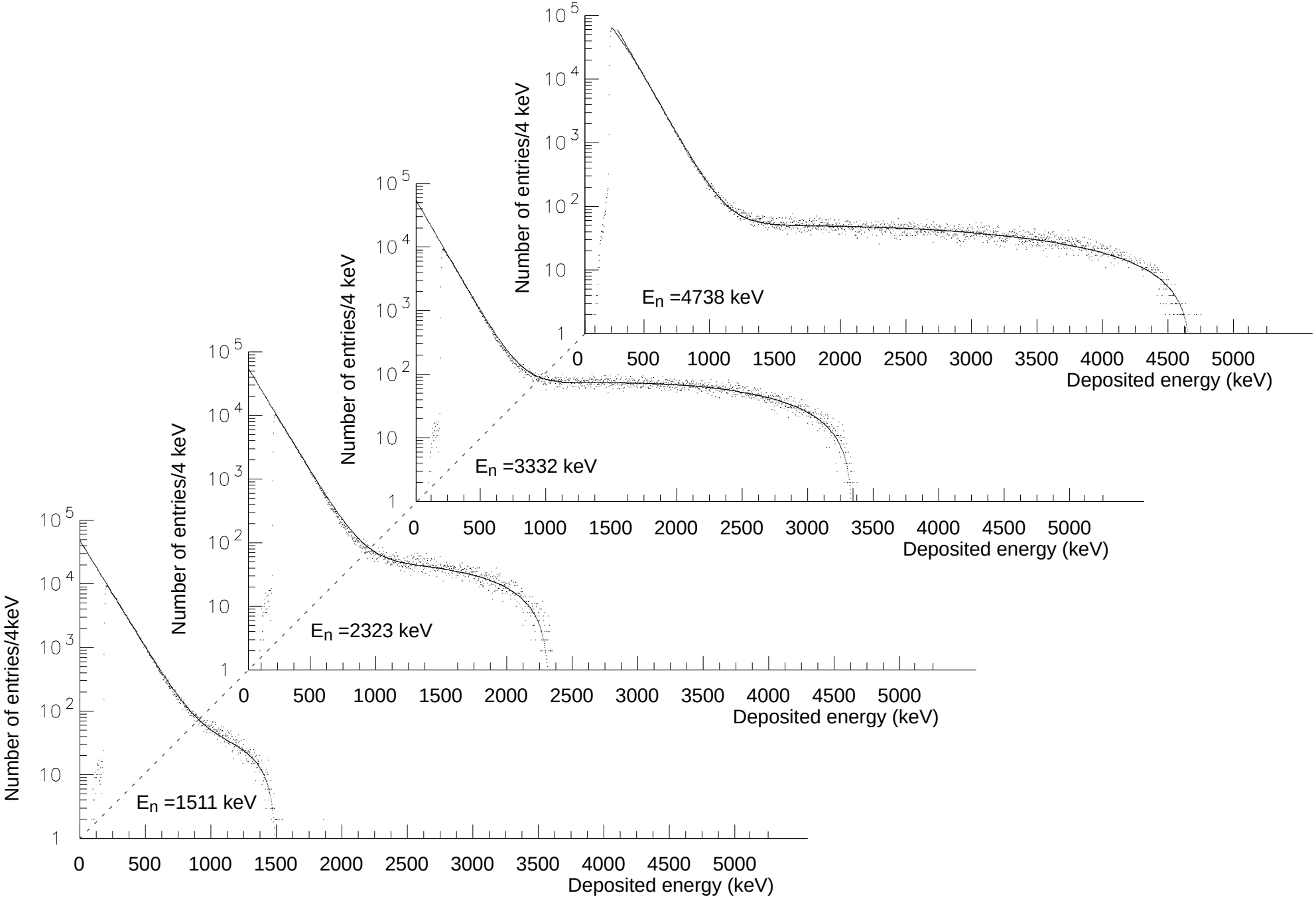
Number of entries/4keV
Number of entries/4 keV
Deposited energy (keV)
E_n =1511 keV
E_n =2323 keV
E_n =3332 keV
E_n =4738 keV
0
500
1000
1500
2000
2500
3000
3500
4000
4500
5000
1
10
10^2
10^3
10^4
10^5

Figure 4

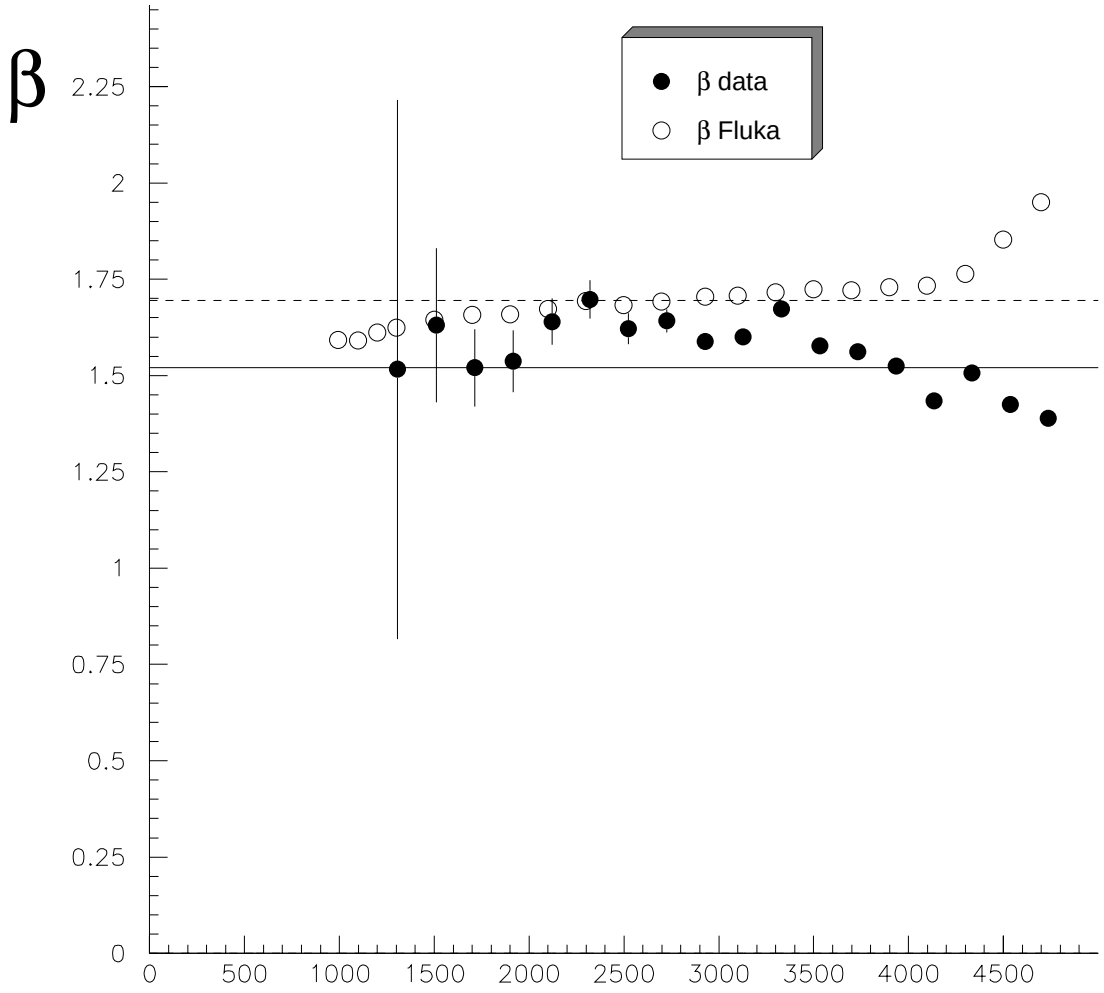

Incident neutron energy E_n (keV)

Figure 5

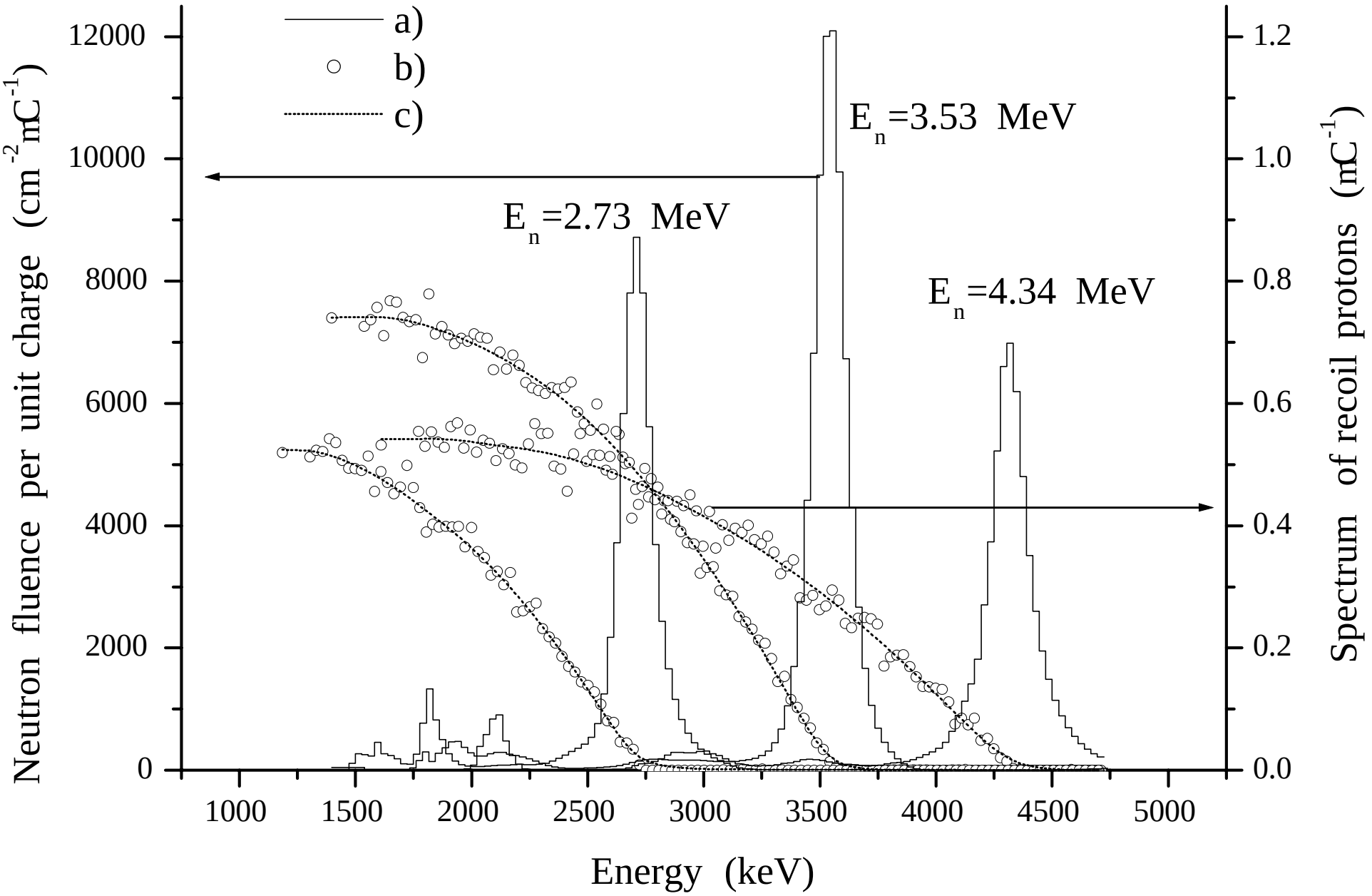
a)
b)
c)
E_n=3.53 MeV
E_n=2.73 MeV
E_n=4.34 MeV
Neutron fluence per unit charge (cm^-2 mC^-1)
Spectrum of recoil protons (mC^-1)
Energy (keV)
12000
10000
8000
6000
4000
2000
0
1.2
1.0
0.8
0.6
0.4
0.2
0.0
1000
1500
2000
2500
3000
3500
4000
4500
5000

Figure 6

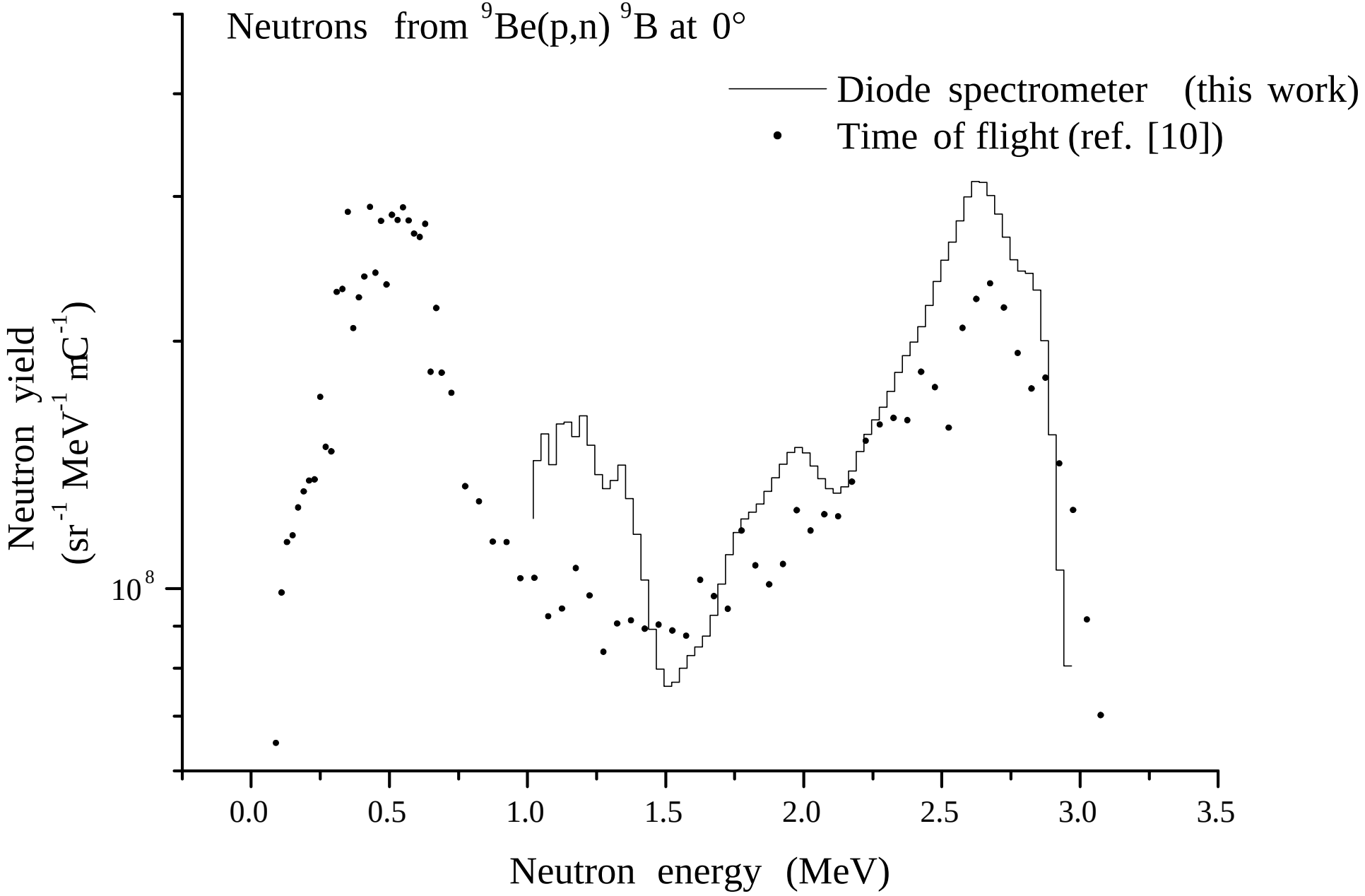
Neutrons from ^{9}Be(p,n) ^{9}B at 0°
Diode spectrometer (this work)
Time of flight (ref. [10])
Neutron yield
(sr^{-1} MeV^{-1} mC^{-1})
10^{8}
0.0
0.5
1.0
1.5
2.0
2.5
3.0
3.5
Neutron energy (MeV)

Figure 7

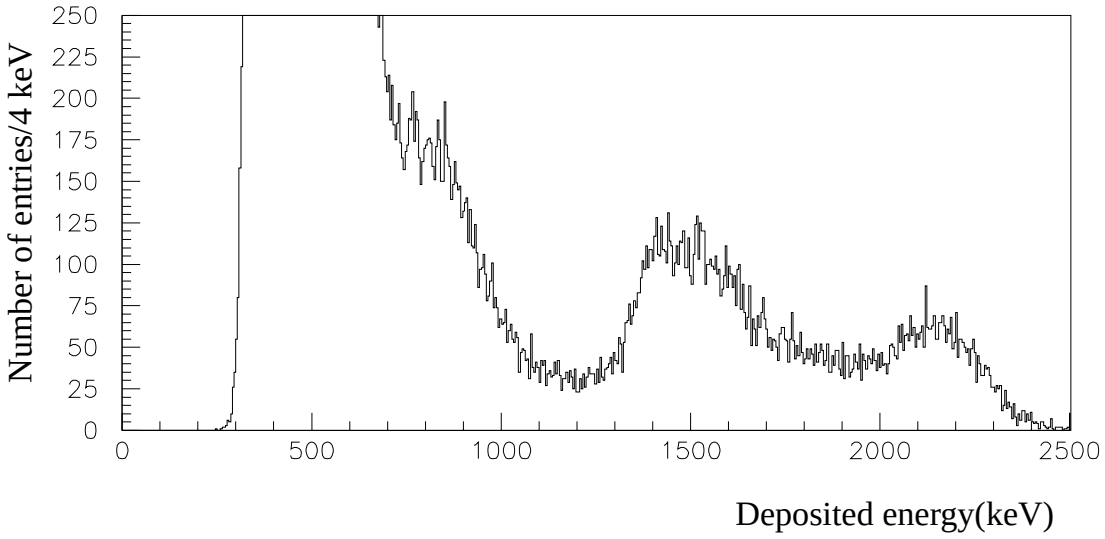
Number of entries/4 keV
250
225
200
175
150
125
100
75
50
25
0
0
500
1000
1500
2000
2500
Deposited energy(keV)

Figure 8

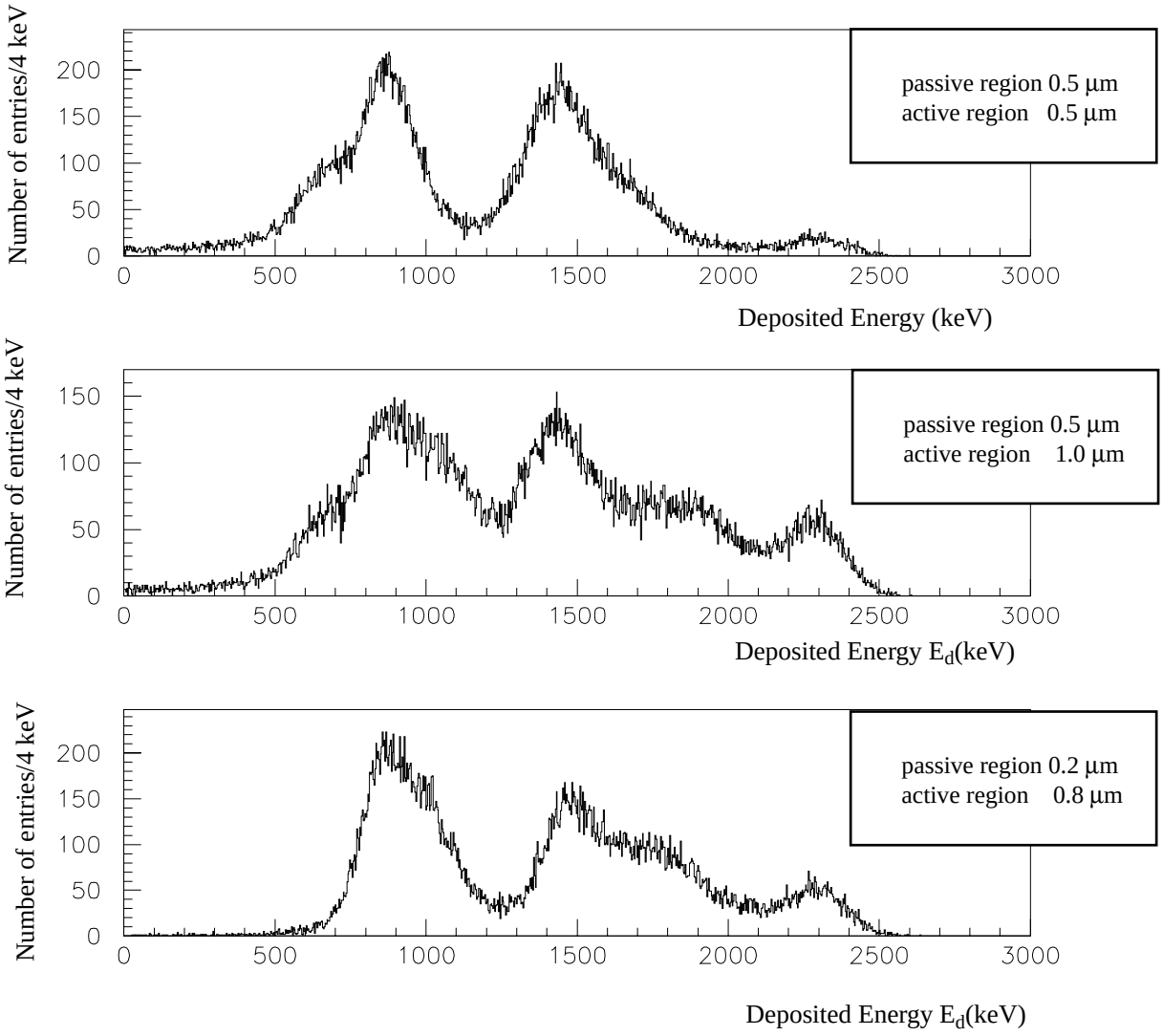
Number of entries/4 keV
200
150
100
50
0
0
500
1000
1500
2000
2500
3000
Deposited Energy (keV)
passive region 0.5 μm
active region 0.5 μm
Number of entries/4 keV
150
100
50
0
Deposited Energy E_d(keV)
passive region 0.5 μm
active region 1.0 μm
Number of entries/4 keV
200
150
100
50
0
Deposited Energy E_d(keV)
passive region 0.2 μm
active region 0.8 μm

Figure 9

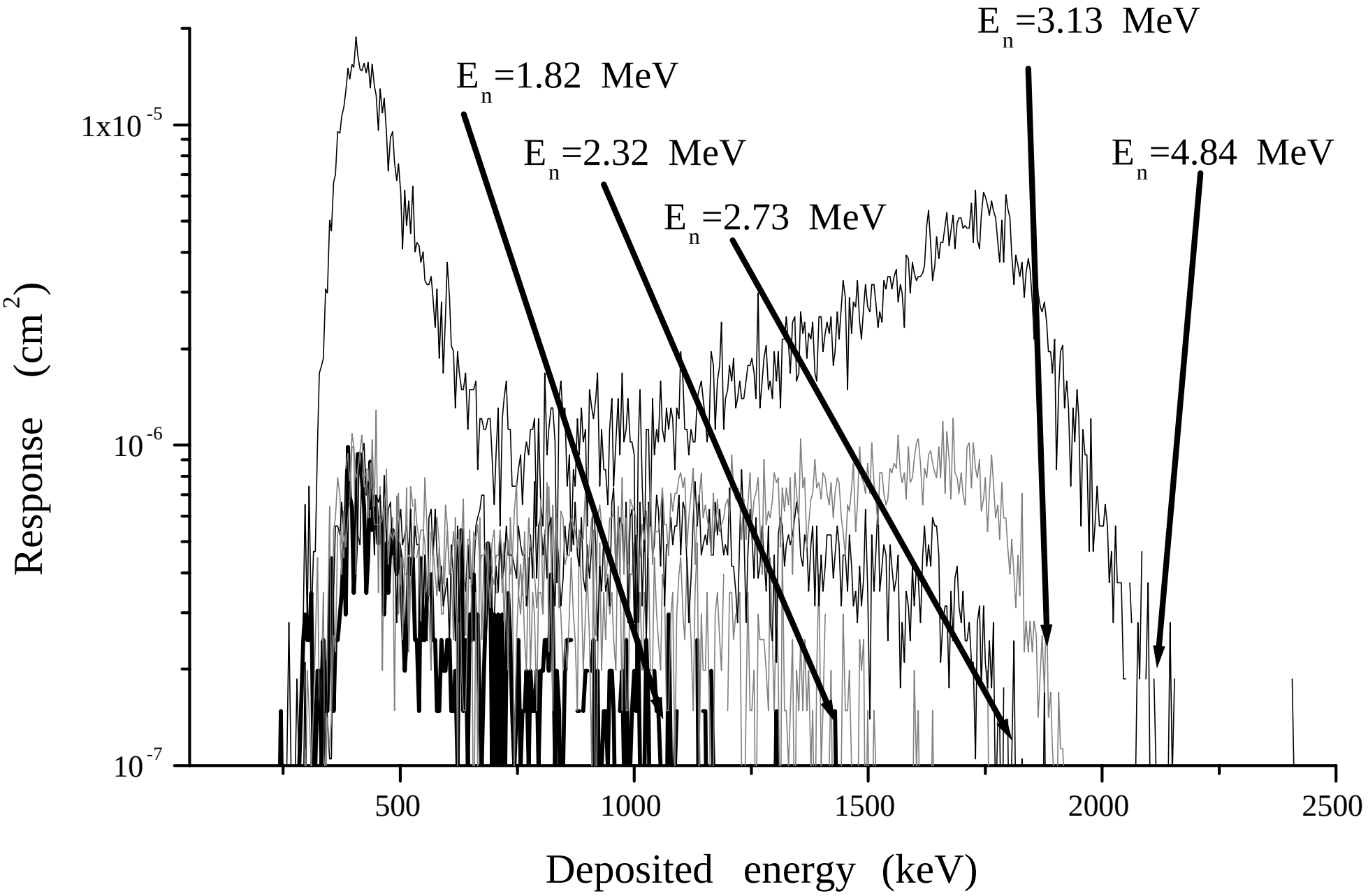
E_n=3.13 MeV
E_n=1.82 MeV
E_n=2.32 MeV
E_n=4.84 MeV
E_n=2.73 MeV
1x10^-5
10^-6
10^-7
Response (cm^2)
500
1000
1500
2000
2500
Deposited energy (keV)

Figure 10

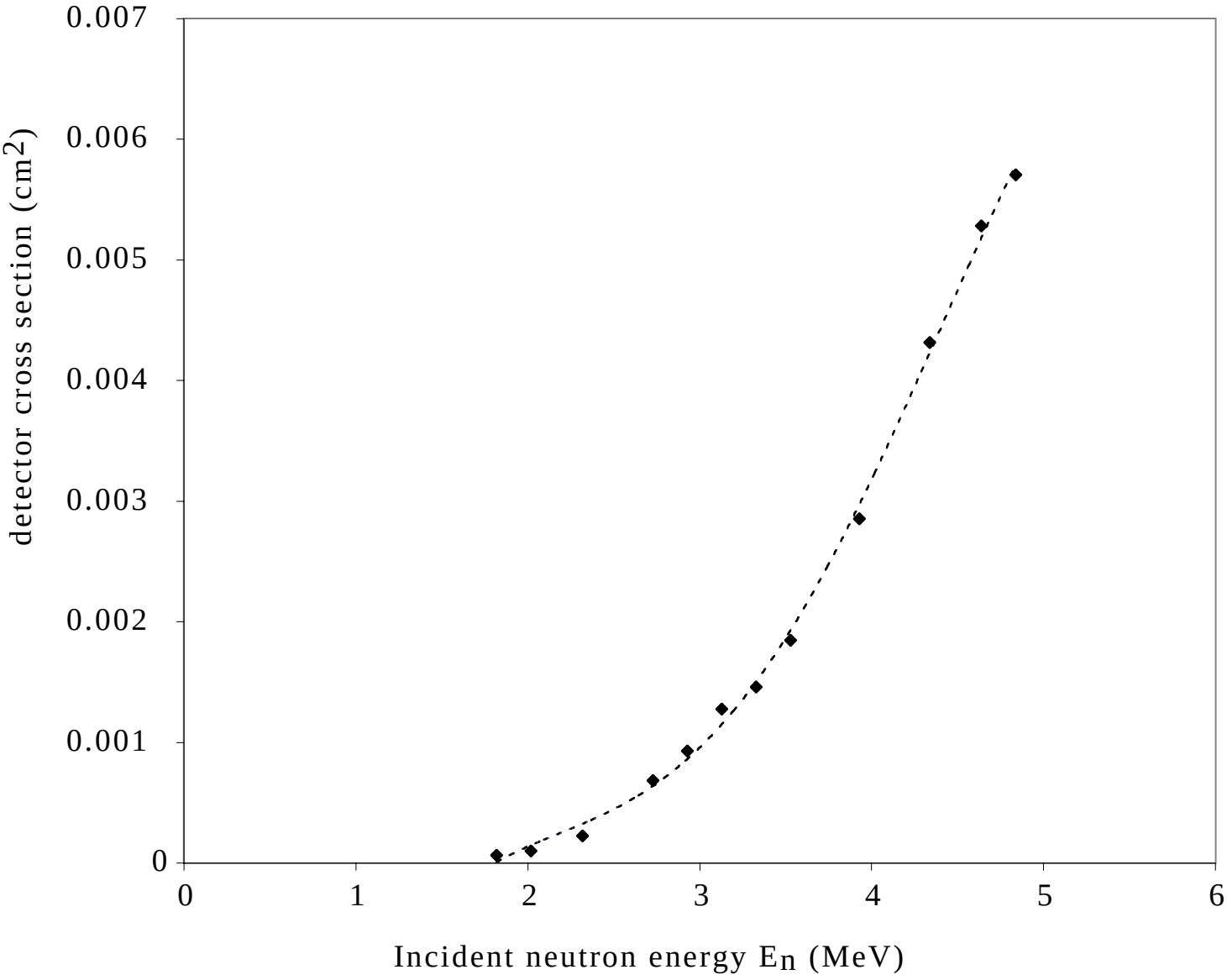
0.007
0.006
0.005
0.004
0.003
0.002
0.001
0
detector cross section (cm2)
0
1
2
3
4
5
6
Incident neutron energy En (MeV)

Figure 11